Reflected Waves in an Inhomogeneous Excitable Medium

G. Bard Ermentrout; John Rinzel

Stable URL:

REFLECTED WAVES IN AN INHOMOGENEOUS EXCITABLE MEDIUM*

G. BARD ERMENTROUT[†] AND JOHN RINZEL[‡]

Abstract. Propagation can be encumbered in an excitable cable in which intrinsic properties change abruptly. A sudden increase in diameter or a decrease in conductivity or excitability can lead to propagation block or delay in propagation with or without reflection. We study such transient phenomena from a geometric point of view. A simple two-cell caricature, with one cell enlarged to mimic diameter increase, is developed and analyzed. Our analysis indicates that reflected waves may result from the existence of an unstable periodic orbit. As the inhomogeneity parameter is varied, this unstable cycle is nearer to and then farther from the initial state that mimics an incoming wave. This fact leads to a variety of complicated reflected waves. Correspondingly, we find numerically complex sequences of reflected-transmitted waves in biophysically more realistic cable analogues. The unstable periodic orbit in the cable appears to be related to a one-dimensional spiral wave described by Kopell and Howard [*Stud. Appl. Math.*, 64 (1981), pp. 1–56]. Finally, we argue that reflection phenomena occur more robustly when excitability is due to saddle-type threshold behavior (type I excitability in the sense of Rinzel and Ermentrout [in *Methods in Neuronal Modeling: From Synapses to Networks*, C. Koch and I. Segev, eds., MIT Press, Cambridge, MA, 1989]).

Key words. echo waves, excitable media, cable equations

AMS subject classifications. 92C20, 92C05, 34B15

1. Introduction.

Cardiac arrhythmic phenomena such as conduction block, reflected waves, and reentry have been studied experimentally using isolated segments of Purkinje fibers and strips of ventricular myocardium. Because of the resistive coupling between cells, one can view these strips as effectively one-dimensional cables of excitable tissue. By using the sucrose gap method one introduces a conduction delay; these delays can be varied by adjusting the shunt resistance, R_s, in parallel with the gap [1, 14]. If the resistance R_s is sufficiently high, conduction block can be obtained. That is, a wave initiated at one end is prevented from reaching the other end. Keener [15] has mathematically analyzed conditions under which conduction block can obtain in spatially discrete excitable media. Another phenomena, seen experimentally for slightly smaller values of R_s, is reflection. If the conduction delay is sufficient for the proximal segment to become repolarized, then when the downstream tissue finally initiates an impulse, the proximal segment, now recovered, becomes reexcited and produces a wave that travels back toward the original stimulus location.

Similar wave behaviors have been demonstrated using ventricular strips treated with increased extracellular potassium in the central segment [23]. We call such a reflected wave an *echo wave*. A geometric analysis of this phenomenon is the subject of the present paper.

Evidence for reflected nerve impulses has also been seen experimentally. An antidromically propagating action potential exhibits conduction delay as it encounters the large change in diameter from the axon to the soma [16]. Ramon, Joyner, and Moore [19] saw partial reflection in a squid axon which had experimentally produced inhomogeneities in conductivity. There have been numerous computer simulations of

---

delayed conduction in models which change the axon diameter or alter local temperature and channel densities. Howe, Calvin, and Loeser [11] obtained fully reflected waves in a chronic nerve injury preparation in rabbit, which has been used as a model for studying the mechanisms of pain. In a computational model, Goldstein and Rall [10] showed that an action potential reaching a sudden large change in diameter will fail to propagate, but for a small range of diameter changes, they found complete reflection. Changes in diameter can also be viewed as equivalent to branching of the axon [10]. Recently, Zhou and Bell [26] have numerically simulated reflected waves in the Morris–Lecar model as part of a study on the effects on inhomogeneities on propagation.

Finally, Chagnac-Amitai and Connors [4] have looked at propagation of activity pulses in a cortical slice preparation treated with bicuculline to suppress fast synaptic inhibition. While the coupling in this tissue is not diffusive as in the previous examples above, it has qualitatively similar properties: it is local and primarily excitatory. With full suppression of inhibitory synapses, wave propagation was robust, without failures or reflections. However, some of their experiments with partial suppression reveal consistent reflected waves or situations in which in some region the activity lingers and is significantly delayed before finally propagating onward. This delay appears to allow the tissue that was previously excited time to recover enough to fire again and thus produce the reflected wave.

We suggest that block and a single reflected wave are part of a large variety of behaviors that can occur at a change in diameter or conductance of an excitable axon (or in any excitable system, for that matter). We call these waves $n{:}m$ echo, where the proximal segment produces n spikes (including the incoming spike that is initiated by the stimulus) and the distal produces m spikes. Thus, conduction block is 1:0, normal transmission is 1:1, and a single reflected wave is 2:1. In addition to these, we will show numerical examples of 2:2, 3:2, and 4:3. We also show that modes that are not of the form $n{:}n$ or $n+1{:}n$ do not appear. In order to motivate these ideas, we begin in §2 with some examples of echo waves: first in a cable, then in a pair of excitable cells, and finally in a simple two variable caricature with dynamics on the torus. The numerical results for a cable suggest that there is an unstable periodic solution that is important for the existence of echo waves. Thus, §3 contains an analysis of the caricature and describes in more detail our conjectured mechanism for the production of echo and $n{:}m$ echo. This section contains the bulk of our paper's mathematics. In particular, we prove that in some circumstances, there is an unstable periodic orbit which we believe plays a pivotal role in the existence of echo waves.

In §4 we compute the unstable periodic solutions that underlie the echo behavior in our biophysical cell models for the cases of two-cell and six-cell chains. We conclude in §5 with a discussion and some possible consequences of this behavior for the production of ectopic pacemakers in nerve axons and cardiac tissue.

2. Blocking, transmission, and intermediate behavior. In Rinzel and Ermentrout [22], we describe some basic properties of excitable cells. In particular, we show that there are two different basic mechanisms for excitability: type II and type I. In type II excitability, found in the familiar Hodgkin–Huxley equations [12], there is a single globally stable equilibrium point, and the threshold is due to the slow dynamics of the recovery variable. It is not a "sharp" threshold in that as the initial condition varies, so does the spike amplitude. (This smooth change in amplitude can be extremely sharp and and will often be noticed only for extremely detailed initial data explorations.) Type I excitability, which is the mechanism underlying the

Goldstein–Rall [10] equations (for which echo has been convincingly demonstrated) as well as the Morris–Lecar equations [18] and the Wilson–Cowan equations in the "active transient" regime [24], is characterized by the existence of three equilibria: an unstable node/vortex (U), an asymptotically stable rest point (R), and a saddle point with a one-dimensional stable manifold serving as the threshold separatrix (T). (In n-dimensional systems, this manifold is an $n-1$ dimensional invariant set.) The threshold for type I excitability is sharp in that the spike amplitude is not continuously graded with the initial condition. Rather, there is a precise threshold (T's stable manifold), and the latency to firing can be arbitrarily long. We will use the Morris–Lecar model for excitability in a regime in which it is of type I. In the discussion section, we briefly consider type II membranes.

2.1. Continuous cable. Consider an excitable cable in which the diameter varies between $d = d_1$ on the left and $d = d_2 \geq d_1$ on the right. In Figure 2.1, we depict the solution to such a cable using the Morris–Lecar membrane model (which is a Hodgkin–Huxley-like two component system and whose equations can be found in the appendix.) In Figure 2.1(a), the difference in the diameters is small so that the impulse which is initiated at the left, propagates through the entire cable. In Figure 2.1(b), the diameter change is too great and propagation is blocked. We can assign indices to these two solutions, calling normal propagation 1:1 and blocked propagation 1:0. The first digit refers to the number of times that the thin cable is excited, and the second refers to the number of times that the thick cable is excited. It is a straightforward numerical task to determine what the ranges of diameter are for block and transmission. For the present model with thin diameter, $d_1 = 1$, block occurs for thick diameter $d_2 > d^* \approx 1.483$ and normal transmission occurs for $d_2 < d_* \approx 1.4102$. Thus, there is a range of diameters in which neither block nor 1:1 transmission occurs. Figure 2.1(c) shows a solution for $d_2 = 1.45$ in which a reflected wave is produced. We call such a wave "echo" and give it an index of 2:1.

It is clear from the simulations above that as the diameter, d_2, continuously varies, there are apparent jumps in the behavior from 1:1 to 2:1 to 1:0. An obvious question is, how does this index change as the diameter varies? In Figure 2.2, we sketch an exaggerated summary of the numerical experiments that we have performed on the cable as the diameter changes. As the diameter increases (toward the blocked case), a sequence of the form 1:1, 2:2, 3:3, and so on occurs until a critical diameter, $d_2 = d_p$, is reached. As one decreases the diameter from the blocked case $(d_2 \geq d^*)$ toward the normal transmission, a sequence of the form 1:0, 2:1, 3:2, and so on occurs until the critical diameter is approached from above. The intervals of each of these indices get smaller and smaller as the number of firings increases. The limiting value of the diameter, d_p, forms the boundary between equal firings of the left and right cable halves and unequal firings. For $d < d_p$ both halves of the cable produce an identical number of spikes; for $d > d_p$ the left half produces precisely one more spike. Thus, it appears that at the critical diameter, there is a periodic solution to the cable in which spikes are alternately emitted from the center of the cable. We expect that this periodic solution exists for a wide range of diameters, however, it is only at the critical value of the diameter that a travelling pulse initiated at the left end "lands" precisely on the cycle. That is, the periodic solution is unstable, and thus only initial conditions that are on the cycle's stable manifold will lead to sustained rhythm. The conjectured unstable periodic orbit is itself interesting as it appears to produce alternating left and right moving waves originating from the point of the inhomogeneity. By adjusting the diameter, we are able to perturb this unstable periodic so that the transient wave
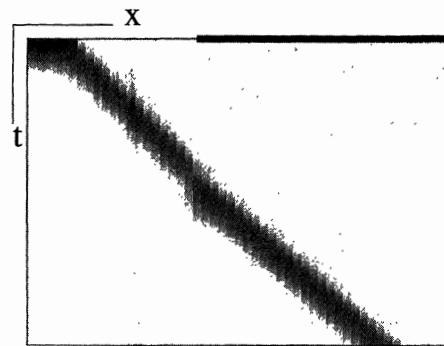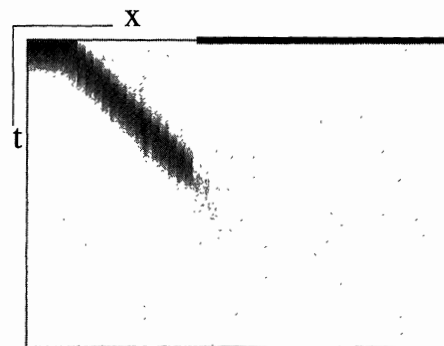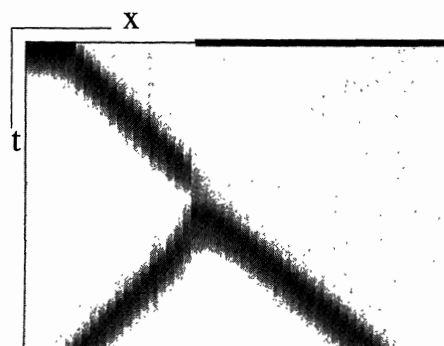
FIG. 2.1. *Numerical solution of a Morris–Lecar cable (see Appendix) which has an abrupt diameter increase. Top border shows diameter change.* $\Delta x = 1$, $\Delta t = 0.1$, $d_1 = 1$, *length of cable is 50. Grey scale indicates voltage.* (a) $d_2 = 1.3$: *normal transmission;* (b) $d_2 = 1.6$: *blocked transmission;* (c) $d_2 = 1.45$: *reflected wave.* (*We obtain similar behavior with finer spatial discretizations; for computational speed, we have purposely kept* Δx *large. All simulations were done using the method of lines and a second-order Euler scheme. Initial conditions for the Morris–Lecar simulations are the resting state* ($v = -0.28$, $w = 0.005$), *except for the stimulated region or cell.*)
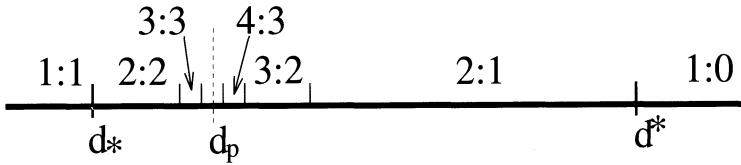
FIG. 2.2. *Sequence of reflected waves as the diameter, d_2, of thick segment varies. Reflected waves occur for $d_* < d_2 < d^*$; block occurs for $d_2 > d^*$. d_p denotes the diameter at which there are infinitely many reflected waves for the particular stimulus of an incoming wave.*

produced by stimulating the thin end of the cable comes close to the unstable periodic. Depending on how close we get, we can produce arbitrarily many reflected waves. In Figure 2.3, we show some of the "exotic" examples of reflected waves.

Our goals in the ensuing sections are to introduce a simplified version of the cable and to use this version to prove that there is such a periodic solution and that it has the property of separating the equal and unequal pulse states. We then show how
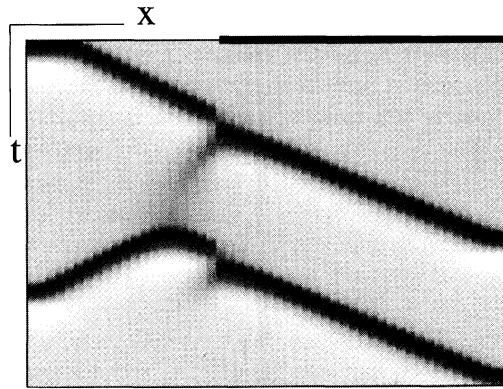
(a)
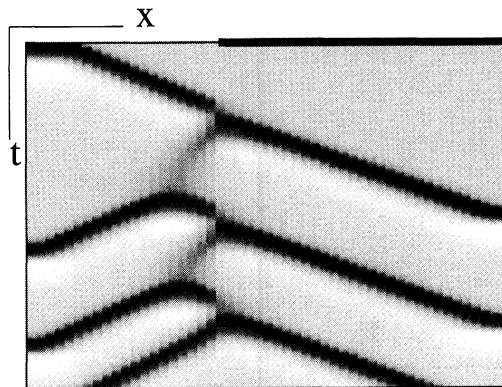
(b)

FIG. 2.3. *"Exotic" reflected waves.* (a) $d_2 = 1.410205$, *2:2 waves;* (b) $d_2 = 1.410207$, *4:3 waves.*

changing the diameter moves this periodic orbit so as to cause block, transmission, and the echo solutions from a single pulse-initiating stimulus.

2.2. Two-cell model. To get a handle on the cable's behavior, we drastically idealize it as a two compartment model with asymmetric coupling. This simplification is representative of either a cable with a changed diameter or one with a region of reduced conductance.

Consider a pair of identical Morris–Lecar oscillators that are diffusively coupled:

$$(2.1) \qquad dv_i/dt = -g_{Ca}m_\infty(v_i)(v_i - 1) - g_l(v_i - v_l)$$
$$- g_k w_i(v_i - v_k) + i + (g_c/d_i)(v_j - v_i),$$
$$(2.2) \qquad dw_i/dt = \phi\lambda_w(v_i)(w_\infty(v_i) - w_i).$$

Here $d_1 = 1$, and $d_2 \geq 1$ is the relative size of the larger cell. g_c is the effective coupling conductance and will be fixed, letting d_2 vary. Parameters are chosen so that in absence of coupling each "cell" has three equilibria: a stable rest state, a saddle point, and an unstable node. The phase plane is shown in Figure 2.4. Recall that this is different from the phase plane for the Fitzhugh–Nagumo equations which have only a single equilibrium value. Differences between the Morris–Lecar system and other excitable systems are described in Rinzel and Ermentrout [22]. The important feature of the present model is the ability of the cell to stay near threshold for an arbitrarily long time before firing. This is due to the presence of the saddle point; initial data close to it will remain nearly constant before traversing the phase plane and emitting a spike. Suppose that both cells are at rest and the first cell is stimulated sufficiently to elicit a spike. If d_2 is too large, then the second cell will not fire and the analogue of block occurs. If d_2 is close to 1 (and g_c is large enough), then the second cell will fire. It is easy to imagine that, like the cable, the values at which block and normal transmission occur are not synonymous. Rather there is a gap in which complex $n{:}m$ firing patterns may occur. Thus, to create the analogy of a pulse incoming from $x = -\infty$, we fix the initial condition of the first cell to be above threshold and the second to be at rest, and let d_2 vary. In Figure 2.5, we show solutions to the coupled system for $g_c = 0.16$ and $d_2 = 2, 1.9436$, and 1.9433 producing 2:1, 3:2, and 2:2 echo, respectively. Keeping in mind that d_2 is proportional to the diameter of the second
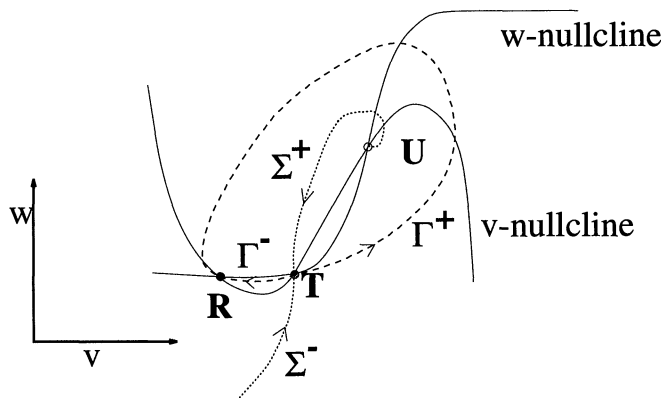

FIG. 2.4. *Phase plane for Morris–Lecar system, showing threshold for excitability and three equilibria.*
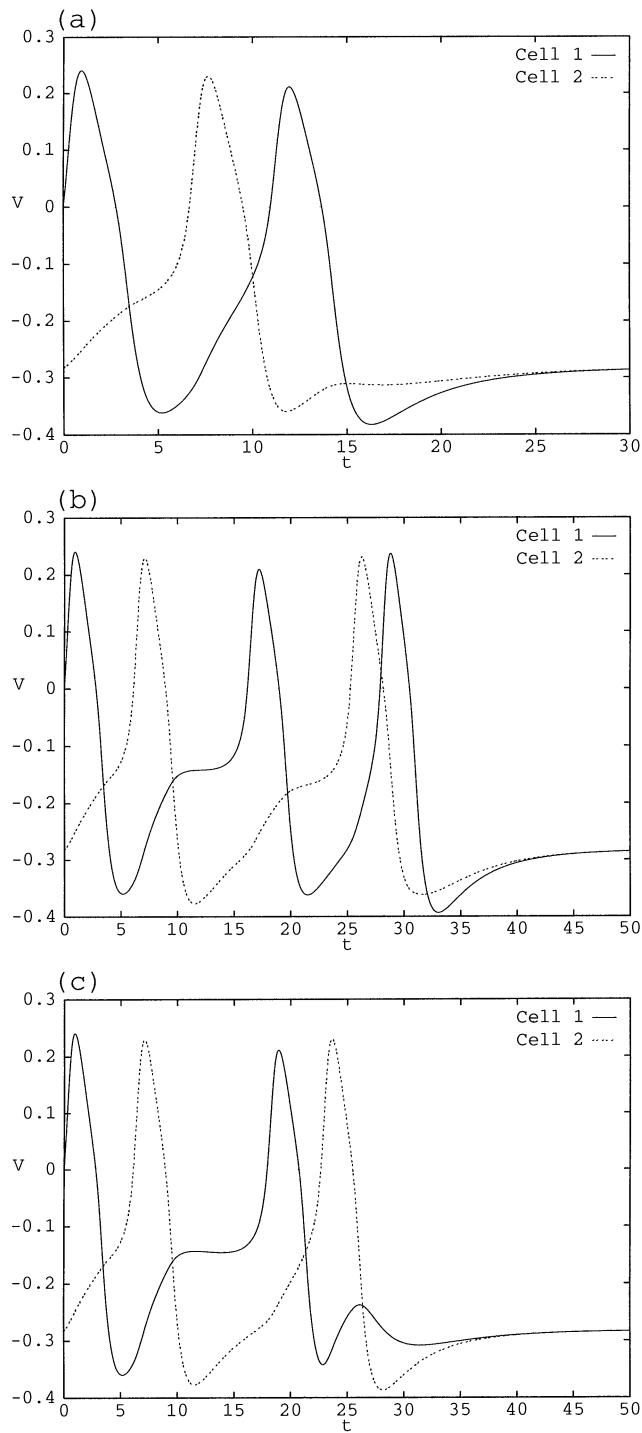
FIG. 2.5. *Voltage time courses for echo and other transient solutions to the two-cell Morris–Lecar model,* (2.1). (a) 2:1 *solution, echo* ($d_2 = 2$); (b) 3:2 *solution* ($d_2 = 1.9436$); (c) 2:2 *solution* ($d_2 = 1.9433$).

cell, we obtain exactly the same sequence of firings as we found in the cable. The intuition is clearer with the two-cell model. The second cell is excited by the first cell but remains close to its threshold long enough for the first cell to recover from firing. When the second cell finally fires, it is able to cause the first cell to fire again, and the two-cell analogue of echo occurs. Preliminary results on this two-cell model were first described in [20].

In the present model for excitability (type I excitability) there is an attracting invariant circle corresponding to the unstable manifold of the saddle point (cf. Figure 2.4). Now suppose that cell 1 fires and cell 2 does not fire for some value of d_2, but for a smaller value of d_2 both cells fire. One can say that cell 2 went from a winding number of 0 to a winding number of 1 in that in the former case it does not traverse the phase plane but in the latter it does. If we suppose that this invariant circle persists, then there are two ways that this transition can occur. The time of firing of the second cell can be arbitrarily delayed, or the impulse of the second cell can continuously grow in amplitude. If the invariant circle persists and is strongly attracting, this latter case cannot occur. If the firing is arbitrarily delayed, then there will be time for the first cell to recover so that it will produce a second spike, i.e., echo. Thus, we believe that there are two important parts to the picture. First, there must be a range for the inhomogeneity parameter values such that a transition from block to transmission occurs. Second, the excitability must be such that the trajectory of the excited cell makes a well-defined loop around the phase space.

2.3. Two-cell phase model. In order to put this rather heuristic argument on firmer mathematical ground, we introduce an even simpler model for an excitable medium. In Figure 2.4 there is a stable circle consisting of the two branches of the unstable manifold of the saddle. On this circle are two equilibria, one stable (the rest state) and one unstable (the threshold saddle point). Thus we consider a model for excitability in which the phase space is the circle:

$$(2.3) \qquad\qquad d\theta/dt = f(\theta),$$

where $f(\theta)$ has a pair of roots, R the stable rest state and T the saddle point threshold. To mimic coupling of two such cells, we introduce a periodic coupling function that depends on the phase difference between the two cells:

$$(2.4) \qquad\qquad d\theta_1/dt = f(\theta_1) + \gamma c(\theta_2 - \theta_1),$$
$$d\theta_2/dt = f(\theta_2) + (\gamma/\delta)c(\theta_1 - \theta_2).$$

The function $c(\phi)$ has the property that $c(0) = 0, c'(0) > 0$, and c has precisely one local maximum and one local minimum in the interval $[0, 2\pi)$. This implies that there is another root, ζ, such that $c'(\zeta) < 0$. The two parameters γ and δ are positive. When $\delta = 1$, the coupling is symmetric. For $\delta > 1$ the model is equivalent to a small proximal cell (cell 1) connected to a large distal cell (cell 2).

Phase models for excitability have been used succesfully in explaining a variety of nonlinear phenomena such as autonoumous bursting [2] and travelling waves in excitable media [25, 9]. When the invariant circle is strongly attracting, they are a good approximation of the full dynamics.

For the purposes of illustration, we choose the following functions:

$$(2.5) \qquad\qquad f(\theta) = 1 - \alpha\cos\theta,$$
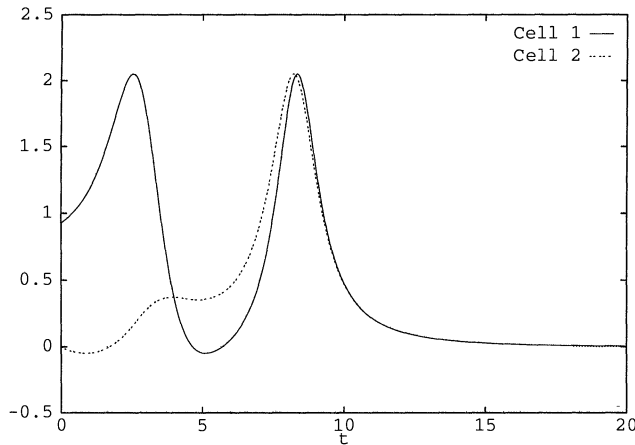$$(2.6) \qquad\qquad c(\phi) = \sin(\phi + \eta) - \sin(\eta),$$

FIG. 2.6. *"Echo" in the phase model. Cell 2 starts at the stable rest state ($\bar{\theta} \approx -.309$), and cell 1 starts at $\theta_1 = 1.5$. Parameters are $\alpha = 1.05, \gamma = 0.8$, and $\delta = 1.25$. Rather than plotting the phases, we plot $1 - \alpha\cos(\theta_j)$ to make the similarity to Figure 2.1(c) more explicit.*

where $\alpha > 1$ and $|\eta| < \pi/2$. When $\eta = 0$, the coupling is particularly simple to analyze and we will keep $\eta = 0$ throughout the remainder of the paper. In keeping with our previous pictures, we fix the initial data of the first cell to be suprathreshold and that of the second cell to be at rest. Then, we vary the parameter δ until block and normal transmission occur.

In Figure 2.6, we show an echo solution to this system of equations. The trajectory traverses one full period around θ_2 and nearly two around θ_1. Each circuit corresponds to the firing of one "spike." Note the long delay in the firing of cell 2. In the next section, we analyze (2.4). For definiteness, when we say "firing" for the phase model, we mean that θ crosses π as that is when $d\theta/dt$ is maximal.

3. Analysis of the phase model. We continue our discussion of the simple phase model described in section 2. We will show that under reasonable assumptions there is an unstable periodic solution to (2.4). The two branches of the unstable manifold of this invariant circle divide the phase space into regions within which each cell traverses the circle a set number of times before returning to rest. Thus, echo is associated with the existence of this unstable periodic orbit. It is interesting to note that the unstable circle persists even in the case where $\delta = 1$, i.e., the cells are identical. In a later section, we numerically show that this is also true in a chain of two or more excitable cells.

Recall that the function $f(\theta)$ has two roots, R and T, corresponding to the stable rest state and the unstable threshold, respectively. Since the coupling function vanishes at zero phase-difference, this implies that there are at least two equilibria for the coupled system corresponding to symmetric solutions $\theta_1 = \theta_2$. We denote these symmetric solutions as (R, R) and (T, T). The following characterizes their stability.

PROPOSITION 3.1. *For γ, δ nonnegative, (R, R) is an asymptotically stable equilibrium and (T, T) is unstable for (2.4).*

Proof. The Jacobian matrix for (2.4) is

$$(3.1) \qquad J = \begin{pmatrix} f'(\bar{x}) - \gamma c'(0) & \gamma c'(0) \\ (\gamma/\delta)c'(0) & f'(\bar{x}) - (\gamma/\delta)c'(0) \end{pmatrix},$$

where $\bar{x}$ is one of R, T. We note immediately that $(1,1)^T$ is an eigenvector with eigenvalue $f'(\bar{x})$. This implies that (T, T) is always unstable since $f'(T) > 0$. Since the sum of the eigenvalues is the trace, the other eigenvalue is $f'(\bar{x}) - \gamma(1/\delta + 1)c'(0)$ so that (R, R) is always a stable node with two negative eigenvalues. For small coupling ($\gamma \ll 1$), the other eigenvalue for (T, T) is positive so that this equilibrium is an unstable node. At a critical coupling strength $\gamma_1 = f'(T)/((1/\delta + 1)c'(0))$, there is an exchange of stability bifurcation and the unstable node becomes an unstable saddle point. We will use this below.   □

If δ is very large and if γ is not too large, then block occurs and there are four equilibria. Indeed, for $\gamma = 0$ there are the two asymmetric equilibria, (R, T) and (T, R), which persist for nonzero values of γ. By letting δ decrease from a very large value, a sequence of bifurcations arises as shown in Figure 3.1. For large δ there are four equilibria with two asymmetric saddles (Figure 3.1(a), (b)). The stable and unstable manifolds of the two asymmetric saddle points break up the phase space in such a way as to make it impossible for any initial condition along the line $\theta_2 = R$ to traverse the circle along θ_2. As the δ decreases toward 1, one of the asymmetric saddles exchanges stability with the symmetric unstable node, becoming a node and leaving the symmetric fixed point, (T, T), as a saddle (Figure 3.1(b), (c)). Further
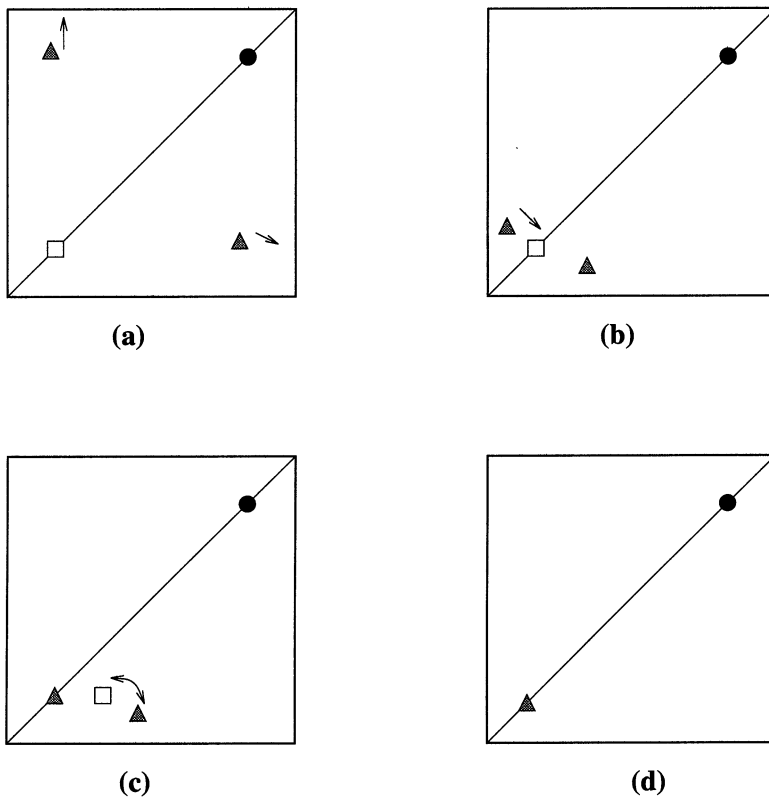

FIG. 3.1. *Sequence of equilibria in $\theta_1 - \theta_2$ plane for (2.4) as a function of decreasing diameter, δ, assuming that γ is in the appropriate range. Point types: stable node, filled circle; unstable node, open square; saddle, filled triangle. Unstable periodic cycle appears when asymmetric saddle and asymmetric unstable node coalesce and disappear.*

decreases in δ toward 1 cause the two asymmetric equilibria to merge in a saddle node bifurcation (Figure 3.1(d)). For all smaller values of δ there are only two rest states: (T,T) and (R,R). This picture is critical to the remainder of our analysis, for here we prove that there exists an unstable periodic orbit that has the property that it winds around both θ_1 and θ_2. This will turn out to imply that there is echo.

Remark. Decreasing the second cell's diameter in the phase model is related to our method for finding echo in the cable and coupled-cell models; start with block and gradually decrease the diameter.

PROPOSITION 3.2. *Suppose that the only equilibria for (2.4) are the symmetric stable node (R,R) and the symmetric saddle point (T,T). Then there exists at least one repelling periodic orbit that traverses the torus with rotation number 1.*

Proof. The diagonal $\theta_1 = \theta_2$ is attracting so that there is a neighborhood around this diagonal out of which no trajectories can flow. If this diagonal strip is removed from the torus, the result is a cylinder containing no equilibria and out of which all trajectories flow. This is topologically a repelling annulus, and in reverse time it follows from the Poincaré–Bendixson theorem that there is at least one periodic orbit. Furthermore, the orbit has a rotation number of 1; both phases wrap around precisely once. (See Figure 3.2.) □

If we now assume that there is an unstable periodic orbit and that it has the property that it wraps around the torus in a 1:1 fashion, then the mechanism for echo becomes clear. In Figure 3.3, we depict an exaggerated view of the two branches of the stable manifold of the symmetric saddle point (T,T) as well as their limit set, the periodic orbit. Call these branches Γ_L and Γ_R, corresponding respectively to the branch emanating from the left and right of (T,T). Consider a horizontal line through the stable rest state. Initial conditions on this line correspond to fixing cell 2 at rest and letting the initial conditions on cell 1 vary. The intersections of Γ_R and Γ_L with this line divide the initial conditions into a sequence of open sets that have special properties. We will use the notation $\vec{ab}$ to denote the curve on the torus corresponding to $\theta_2 = R$ and $\theta_1 \in (a,b)$. Suppose that we start in the set $\vec{R0}$. Following the trajectory we see that neither cell fires. This corresponds to block of the firing of both cells. We call this 0:0 echo. Note that this region extends beyond the threshold for firing cell 1 in the absence of coupling. Intuitively, the "current drain" due to coupling increases the threshold for firing the first cell. Suppose that we now start in region $\vec{01}$. This results in both the firing of cell 1 and the firing of cell 2 and is called 1:1 echo or normal transmission. Initial conditions in region $\vec{12}$ result in two firings of each cell, or 2:2 echo. Indeed, in each of the regions to the left of the critical periodic orbit, we obtain n:n echo for nonnegative integers n.

Let us turn to the regions to the right of the critical orbit. Consider initial data in the region $\vec{6R}$. Following this trajectory we see that cell 1 fires once and cell 2 does
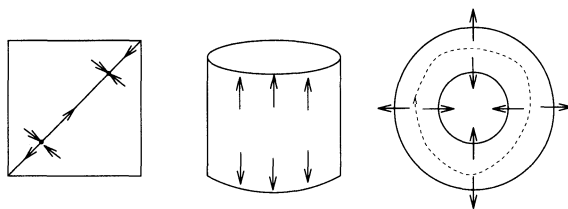

FIG. 3.2. *Deformation of the torus with the diagonal removed to form an annulus.*
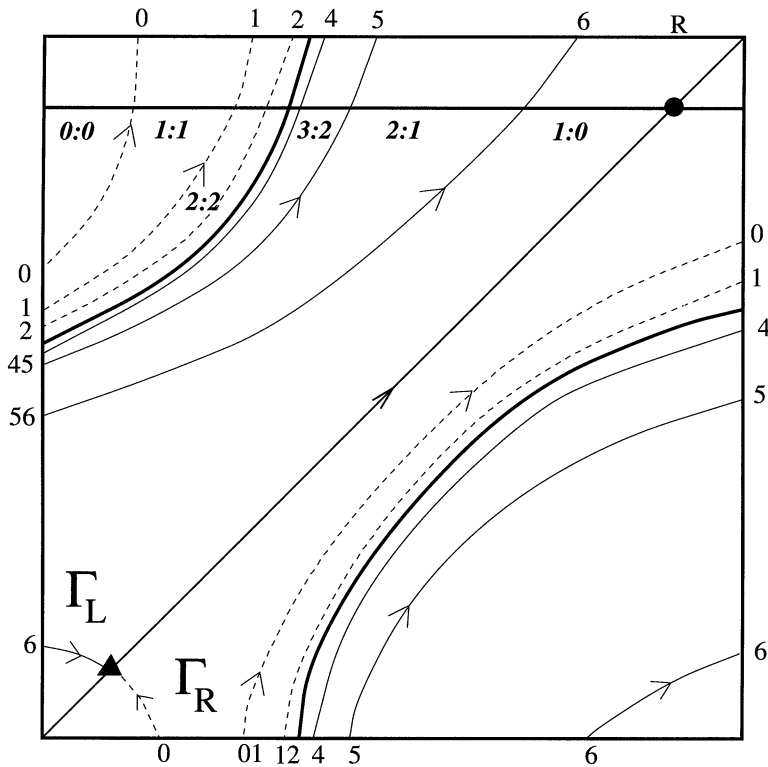
FIG. 3.3. *Exaggerated view of the phase plane picture corresponding to echo for the two-cell phase model. The numbers are meant to aid in identifying the trajectories on opposite edges of the torus. Numbers along the top also serve to define the endpoints of the intersections with the line $\theta_2 = R$. Double numbers along the left and bottom edges associate numbers on the right edge with those on the top edge. The unstable periodic orbit is the heavy curve.*

not fire at all. This is called 1:0 echo and corresponds to the usual notion of block. Next let the initial data lie in $\overline{65}$. The result is that cell 1 fires twice and cell 2 fires once. We have found 2:1 echo, which is the usual notion of a reflected spike. As we move closer to the critical orbit, more and more firings are added; as long as we remain to the right, there will be $(n + 1):n$ echo for all nonnegative integers, n.

In the above discussion, we have held the parameters fixed and varied the initial data. However, one can just as easily fix initial data and vary the parameters. For a fixed value of the coupling parameter, γ, we can vary δ and plot (Figure 3.4) the boundaries for 1:1 and 1:0 (block). These are simply the first points where the stable manifold of the symmetric saddle point intersects the line $\theta_2 = R$. Initial conditions within this narrow band will lead to 2:1 and more complex echo solutions. Note that intermediate values of δ give the largest range of initial conditions leading to echolike solutions.

Proposition 3.2 shows that under fairly general circumstances there is an unstable periodic orbit. However, it yields little information about the detailed structure of the orbit. The following propositions use singular perturbation theory to explore the quantitative features of this orbit. Furthermore, we can see precisely how the echo behavior disappears through a block solution. Numerical results in the next section confirm that a similar behavior occurs for the two-cell model.
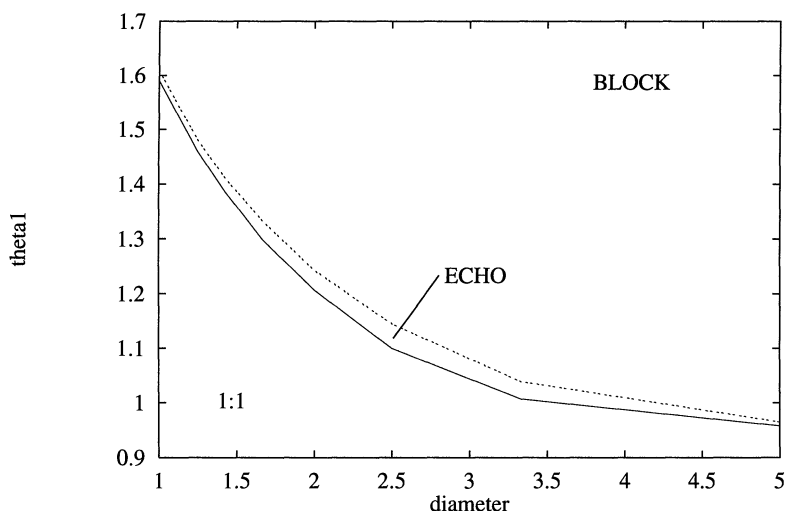
FIG. 3.4. *Region for initial state of cell* 1 *that leads to echolike behavior for* $\gamma = 0.8$, $\alpha = 1.05$ *fixed and diameter,* δ, *variable.*

We first consider the case for which the second root of the coupling function c is not π as it is in the above figures and examples ($\eta = 0$). (When c is an odd function, the second root is π. More generically, the second root will not be π. However, for c odd, the analysis yields more details. Thus, we discuss both cases.) In both cases, we assume that the coupling strength is large. Since any fixed-diameter difference can be overcome with large enough coupling, we will assume that the diameter of the second cell is of the same order of magnitude as the coupling strength. That is, we set $\gamma/\delta = \beta$ and assume that β is $O(1)$ as $\gamma \to \infty$.

PROPOSITION 3.3. *Let* $\phi = \bar{\phi}$ *be the nonzero root of* $c(\phi) = 0$ *such that* $c'(\bar{\phi}) < 0$ *and* $c(-\bar{\phi}) \neq 0$. *Let* $\beta = \gamma/\delta$ *be fixed and positive as* $\gamma \to \infty$. *Then for* γ *sufficiently large,* $\theta_2 - \theta_1 = \bar{\phi} + O(1/\gamma)$ *and*

$$(3.2) \qquad\qquad \theta_2' \approx f(\theta_2) + \beta c(-\bar{\phi}).$$

Proof. To prove this, we will introduce a new coordinate system. Let $\theta_2 - \theta_1 = \bar{\phi} + \xi$ and consider the system in terms of (ξ, θ_2). If we let $\epsilon = 1/\gamma$, we obtain

$$(3.3) \qquad\qquad d\theta_2/dt = f(\theta_2) + \beta c(-\bar{\phi} - \xi),$$
$$(3.4) \qquad\qquad \epsilon d\xi/dt = -c(\bar{\phi} + \xi) + \epsilon(f(\theta_2) - f(\theta_2 - \bar{\phi} - \xi)$$
$$+\beta c(-\bar{\phi} - \xi)),$$

Setting $\epsilon = 0$ we see that $\xi = 0$ is an invariant circle on the torus (ξ, θ_2). This yields the equation, (3.2), for the dynamics on the invariant set. Since $c'(\bar{\phi})$ is nonzero, it follows from [7] that the set is hyperbolic. Thus, it persists for $\epsilon > 0$ and sufficiently small. Furthermore, since $c'(\bar{\phi}) < 0$, the set is repelling.   □

For β small (that is, a large value of the diameter compared to the coupling strength) (3.2) has fixed points. However, since $c(-\bar{\phi}) \neq 0$ as β is increased (i.e., the diameter is reduced), θ_2' will be of one sign and so there will be a nontrivial periodic solution on the torus on which both θ_2 and θ_1 traverse one cycle. This is the unstable periodic orbit of Proposition 3.2. This suggests the following scenario for

the production of echo in the phase model. For a large-diameter cell, there is block. As the block is removed, an unstable periodic arises via a saddle-node loop. This unstable orbit serves as the mechanism by which echo is produced.

Since our numerical examples use $c(\phi) = \sin(\phi)$, we will prove a modification of Proposition 3.3 in which the existence of the unstable circle is guaranteed, but we do not need to assume that the diameter, δ, is of the same order of magnitude as the coupling strength, γ.

PROPOSITION 3.4. *Suppose that $\bar{\phi} = \pi$ and c is an odd function. Then for sufficiently large γ there is an unstable invariant circle, $\theta_2 - \theta_1 = \pi + O(1/\gamma)$, on which the dynamics satisfy*

$$(3.5) \qquad \frac{d\theta_2}{dt} = \frac{\delta f(\theta_2) + f(\theta_2 + \pi)}{\delta + 1}.$$

Remark. Depending on the size of δ, this system may or may not have any equilibria. If there are no equilibria, then θ_2' is of one sign and so there is an unstable periodic orbit. Clearly as $\delta \to \infty$ the right-hand side of (3.5) tends to $f(\theta_2)$, which has a fixed point.

Proof. We once again introduce new variables. Let $\epsilon = 1/\gamma$ and $\theta_2 - \theta_1 = \pi + \epsilon\xi$. Then (2.4) becomes

$$\epsilon\frac{d\xi}{dt} = f(\theta_2) - f(\theta_2 - \pi - \epsilon\xi) - \frac{1}{\epsilon}(c(\pi + \epsilon\xi) + c(\pi + \epsilon\xi)/\delta)$$
$$= f(\theta_2) - f(\theta_2 - \pi) - c'(\pi)\xi(1 + 1/\delta) + O(\epsilon),$$
$$\frac{d\theta_2}{dt} = f(\theta_2) - \frac{1}{\epsilon\delta}c(\pi + \epsilon\xi) = f(\theta_2) - c'(\pi)\xi/\delta + O(\epsilon).$$

Since $c'(\pi) \neq 0$, we can set $\epsilon = 0$ and solve the first equation for ξ. Substituting this into the equation for θ_2 yields the desired equation for (3.5). Since $c'(\pi) \neq 0$, the invariant set defined by ξ is hyperbolic so that it persists for ϵ small and positive. ☐

We have shown that an unstable periodic solution exists and argued that this solution implies that echo occurs in the simple phase models. In the broader context of biophysical models, the existence of the periodic coincides with echolike behavior only in so far as it is the limit of $n{:}n$ and $n+1{:}n$ types of solutions. In the next section, we reconsider the two-cell model and numerically show that there is an unstable antisymmetric periodic solution for parameters in which there is echo.

4. Numerical computation of unstable periodic solutions for nerve membrane models. In the previous section, we suggested that echo solutions arise as the diameter of the "thick" cable decreases from the blocked case, and that these transient solutions are a consequence of an unstable periodic orbit in the dynamics of the coupled system. Here, we use numerical methods to compute this periodic orbit, first for the two-cell Morris–Lecar model and then for a six-cell version. We compute the unstable periodic orbit over a range of diameters, including the case of identical cells. For the two-cell model, we show that the orbit's position in phase space (as a function of d_2) allows us to anticipate whether block, echo, or 1:1 transmission will occur. For the discrete (homogeneous) cable, the unstable periodic orbit appears to be related to the unstable one-dimensional "spiral" waves that were first discovered by Kopell and Howard [17]. In the next section, we show that wave reflection phenomena occur more generally, for other types of inhomogenieties, and even for type II excitability, although less robustly it seems.

4.1. Periodic solutions for the two-cell model. Consider once again the two-cell Morris–Lecar system (2.1). We choose the diameter of the second cell to get a complicated echo (in the present example, 5:4 echo, occurring for $g_c = 0.16$ and $d_2 = 1.94344$). Then we pick a portion of this transient, and use it as a starting guess for the continuation software AUTO [6]. In Figure 4.1 we depict the unstable periodic orbit found by AUTO along with the projection of the 5:4 echo solution in the $v_1 - v_2$ plane. The periodic orbit is indistinguishable from the middle part of the transient echo solution. We can then use AUTO to study the evolution of this orbit as we change the diameter. As d_2 is increased, we find that at $d_2 \approx 3.5523$ the unstable periodic orbit disappears via a saddle-node bifurcation. The periodic orbit persists as d_2 decreases to 1. This is exactly the same scenario as occurred in the two-cell phase model described in § 3.

It is important to emphasize that the existence of the unstable periodic orbit does not imply that echo solutions will occur for the membrane model. Rather, we believe that its existence is a necessary condition for echo. For example, in the above calculation, the unstable periodic persists for $d_2 = d_1 = 1$, but we have never found echo in this regime. The reason is that the trajectory evolving from the initial conditions that we use to mimic an incoming wave (cell 2 at rest and cell 1 at a fixed suprathreshold voltage, $v_2 = 0.0$) never comes close to the unstable orbit. In the blocking regime, the same holds: the initial data are not on a trajectory that comes close to the unstable orbit. Figure 4.2 shows a blown-up region of the $v_1 - v_2$ plane illustrating the trajectories of the unstable periodic orbit for three different diameters. The horizontal line is the curve of initial values of v_1 when v_2, w_1, and w_2 are at rest. The differences between block, echo, and transmission are clearly illustrated. (Note that the middle trajectory is an expanded view of the unstable periodic orbit shown in Figure 4.1.) Block occurs when the unstable orbit lies sufficiently above the
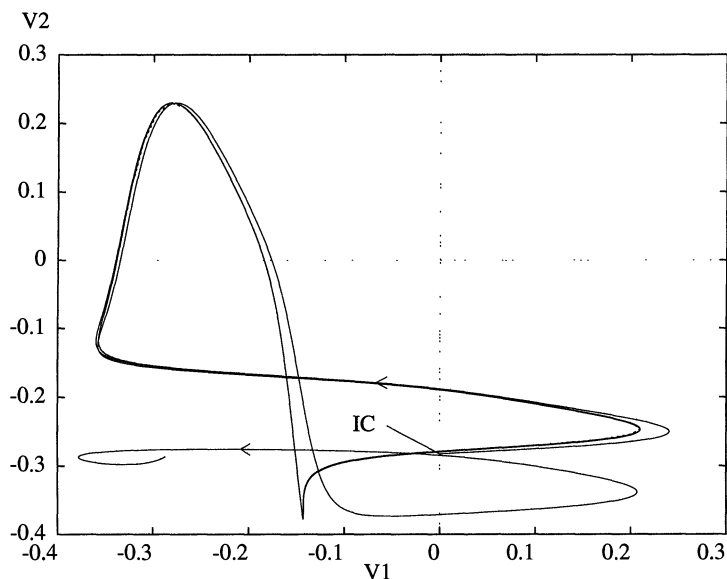

FIG. 4.1. *Voltage plane showing the two-cell unstable periodic orbit (dashed line) and the 5:4 echo solution (solid line). Initial condition for the echo solution is shown (IC). (The dashed periodic orbit is essentially identical to a piece of the echo solution and thus is barely visible in this picture.)*
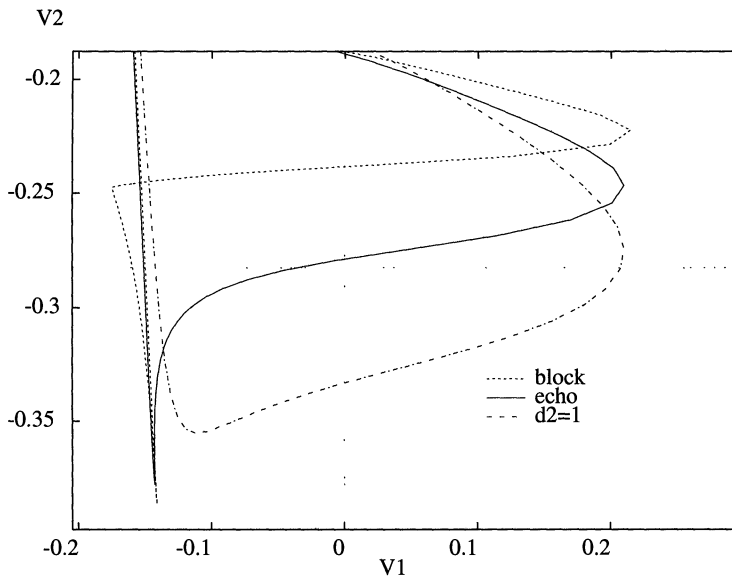
FIG. 4.2. *Voltage plane showing the two-cell unstable periodic orbit for values of d_2 at which there is block ($d_2 = 2.6$), echo ($d_2 = 1.98$), and 1:1 transmission. The horizontal line shows the resting value of v_2, and the vertical line is the initial value of v_1 used to mimic an "incoming" wave.*

"incoming wave" initial conditions, for then cell 2 never gets excited enough to fire. 1:1 transmission occurs when the initial conditions lie sufficiently inside the unstable orbit. The second cell fires easily, but the trajectory is far enough away from the unstable orbit to preclude subsequent firings of either cell. Echo occurs when the initial conditions are close to the unstable periodic orbit. Thus, echo emerges in the two-cell system in the same manner as in the phase model. As we decrease the diameter of cell 2 from a large value, the unstable periodic orbit's $v_1 - v_2$ projection moves downward, and the sequence of "reflected" wave patterns $n + 1{:}n$ followed by $n{:}n$ is seen until the trajectory falls low enough, after which 1:1 transmission is found. The unstable orbit, while existing in regions where there are no echo solutions, plays a pivotal role in the transient behavior of the two-cell model as one goes from block to 1:1 transmission.

Another question that can be asked is, how does this unstable periodic orbit, born as a homoclinic at a saddle-node point, disappear? If we continue decreasing d_2 below unity, then cell 1 is the larger cell and, by analogy, we expect that the orbit ought to become homoclinic and disappear for small enough d_2. It can also be lost in a different way, by varying an intrinsic excitability parameter. Starting with our orbit, continued to the symmetric case of identical cells, we increased the stimulating current I in both cells and used AUTO to follow the orbit. If the current is large enough, each cell individually oscillates. Our unstable periodic orbit is just the expected antiphase solution of two oscillators, coupled with weak diffusion [21]. This feature means the case of two cells is special in some sense. Thus, to get more insight into the origin and role of the unstable periodic in the cable, we turn to a longer chain of cells.

4.2. Multiple-cell periodics. For simplicity, we have numerically investigated a chain of six Morris–Lecar cells with diffusive coupling on v_j. The first three cells have diameter 1, and the last three have diameter d. With coupling $g_c = 0.5$, echo
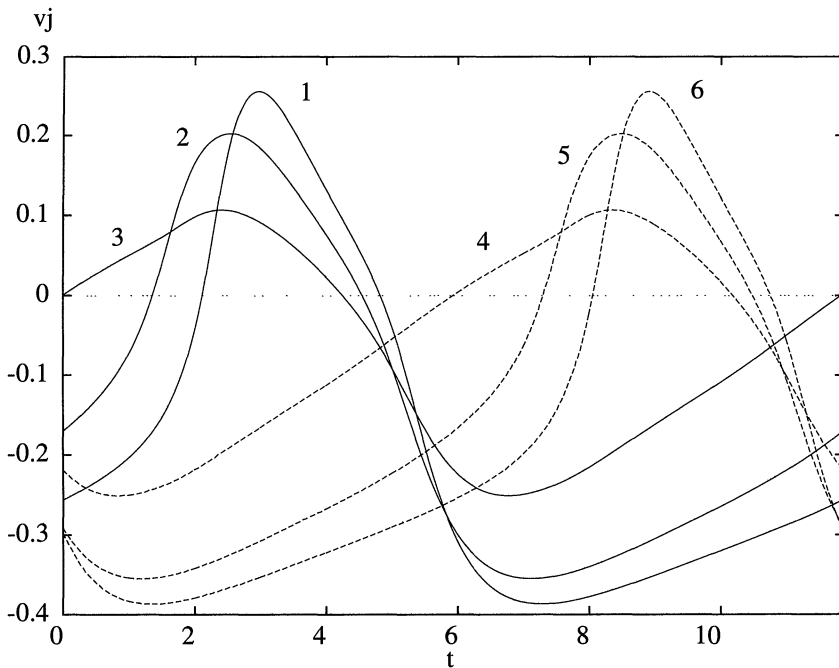
FIG. 4.3. *Unstable periodic orbit for a chain of six Morris–Lecar cells with $g_c = 0.5$. This pattern is the discrete-chain analogue of one-dimensional spiral pattern of Kopell and Howard* [17].

occurs when $d \approx 2.5$ and persists over a wide range of values. Using the methods described above, we can get a good approximation for the unstable periodic at a value of d for which there is echo. Then, using AUTO, we continue this branch back to $d = 1$. Figure 4.3 shows the cells' voltage time courses for the periodic solution at $d = 1$. The left central cell (cell 3) fires and produces a wave going to the left. Half a period later the central right cell (cell 4) fires and produces a rightward wave. This pattern of alternating leftward- and rightward-going waves, emanating from one location, is the discrete-cell analogue of the one-dimensional spiral pattern discovered by Kopell and Howard [17]. The pattern was shown to be unstable by Ermentrout and Rinzel [8]. While the proof of Kopell and Howard was for a very special class of oscillatory reaction-diffusion equations, we believe that these solutions exist in cables more generally. In fact, our cable is excitable, not autorhythmic. Thus, we conjecture that echo on a continuous cable equation is a consequence of an unstable periodic solution that is a continuation of the unstable one-dimensional spiral wave solution centered at the point of the inhomogeneity.

5. Discussion. We have described reflection and block phenomena for coupled-cell pairs, chains, and continuous excitable cables in which parameters such as diameter change abruptly with distance. Figure 2.2 summarizes the complex systematic sequence of echo waves that we believe occurs as the degree of inhomogeneity changes. The mathematical solutions for echo are difficult to analyze since they are transient rather than stable and persistent, as are stable traveling wave solutions, for example. On the other hand, we have gained insight into these behaviors by identifying an underlying persistent structure, an unstable periodic orbit that plays a key role. As we have shown, mere existence of such an orbit, however, does not guarantee echo

behavior; the orbit exists over a parameter range that exceeds the echo range. Of importance is how the specific initial conditions of interest (for us, those that mimic an incoming wave) relate to the unstable orbit. If they lead to a trajectory that comes near the orbit, then echo can occur. As the inhomogeneity parameter is varied, the complex transition from block to 1:1 transmission climaxes for a critical parameter value with an infinite number of reflected and transmitted waves. In mathematical terms, we conjecture that at criticality the initial state lies on the unstable periodic orbit's stable manifold. The manifold sweeps through the incoming wave initial state as the parameter is varied; the $(n + 1){:}n$ and $n{:}n$ behaviors occur when the initial conditions are either "above" or "below" the stable manifold.

This understanding was reached by explicit analysis of the two-cell phase-variable model. The phase model embodies the essence of type I excitability, a saddle-type threshold behavior. We believe this feature underlies robust echo behavior; it is found in several other models that show echo (see introduction). This is not to say that reflections do not occur in a cable having type II excitability. Finding echo with, say, the standard Hodgkin–Huxley equations is possible, but the regime is very narrow. Such type II models, without a sharp threshold, can yield spike responses of graded amplitude as the initial data change. Indeed, when one varies d_2 between regimes of block and 1:1 transmission for the Hodgkin–Huxley equations or the Morris–Lecar equations (in the parameter regime for type II firing) one does find echo in a two-cell model, but for a very narrow range. However, the spike of the second cell is considerably smaller than its usual height because of the "pull" toward equilibrium from the coupling. Figure 5.1 shows an example of "echo" in the two-cell Morris–Lecar system when the dynamics are type II. Note the diminished amplitude of the second cell's spike. In contrast, for the type I case of Figure 2.5(a), the downstream spike has full amplitude. It appears that small ϕ enhances the possibility for type II echo. If the dynamics are not close to the relaxation limit, the transition from block
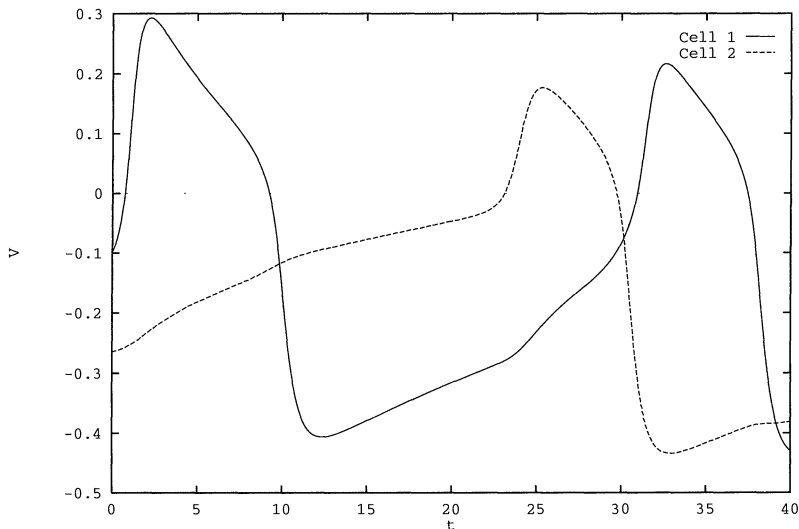

FIG. 5.1. *Voltage traces for echo in a two-cell Morris–Lecar model, with type* II *excitability. Parameters are the same as those in previous figures except* $\phi = 0.1$, $v_3 = 0$, $v_4 = 0.3$, $g_{Ca} = 1.1$, $i = 0.2$, $g_c = 0.2$, $d_2 = 3.79$.

to transmission occurs via a gradual increase in the amplitude of v_2, not in the way we have viewed echo. We finally note that, as in our analysis for type I echo, there is an unstable periodic orbit. Thus, for echo with type II excitability, an unstable periodic orbit still appears necessary.

Up to now, we have discussed echo in the context of changing diameter. Significant inhomogenieties in other parameters can also lead to conduction delays, block, and reflections. In many of the cardiac preparations, propagation is jeopardized in a localized region by a reduced axial conductance. Thus consider, instead of a cable with a changing diameter, one for which there is a reduced conductance over some midportion of its length. As noted in the appendix, this results in a slightly different equation. For illustration, we let the axial conductance decrease by 42% in a interval from $x = 20$ to $x = 24$ on a cable of length 50. As in the case of a changing diameter, there is a reflected wave (Figure 5.2). There is a range, approximately between 40% and 50% conductance decrease, where reflected waves are found.

As noted by Goldstein and Rall [10], the existence of reflected waves suggests a means by which a pacemaker could be created. Consider a long axon with a smaller-diameter central region. Stimulating the left end results in a wave that propagates into the thin region. If a reflected wave occurs on the thin segment after the right thicker region is excited, it will propagate back to the left again, exciting the leftmost segment. A wave is again reflected and travels to the right. This continues periodically and results in a "pacemaker." Similar rhythmogenic phenomena associated with mid-axon changes in properties may be involved with neural mechanisms of pain such as trigeminal neuralgia [3]. Since wave reflection occurs in cellular discrete media as well as in continuous cables it may provide yet another mechanism for ectopic pacemakers in cardiac tissue. Ito and Glass [13] and Chay [5] have suggested that such ectopic pacemakers can arise by reentry in "rings" of cardiac excitable tissue. The mechanism outlined here is geometrically much less stringent and requires only some local inhomogeneities in the fibers.
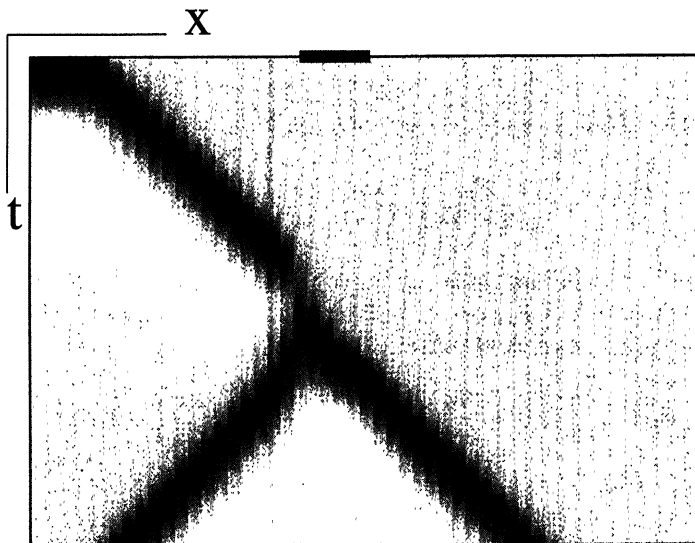

FIG. 5.2. *Echo resulting from a region of decreased axial conductance in a type* I *Morris–Lecar cable.*

Appendix.

A.1. Morris–Lecar equations. The Morris–Lecar model is a simplified conductance-based model with a fast persistent calcium current and a delayed-rectifier potassium current. The dimensionless equations (see [22]) are

$$\frac{dv}{dt} = i - g_l(v - v_L) - g_K w(v - v_k) - g_{Ca} m_\infty(v)(v_{Ca} - v),$$

$$\frac{dw}{dt} = \lambda_w(v)(w_\infty(v) - w),$$

where

$$m_\infty(v) = .5(1 + \tanh((v - v_1)/v_2)),$$
$$w_\infty(v) = .5(1 + \tanh((v - v_3)/v_4)),$$
$$\lambda_w(v) = \phi \cosh((v - v_3)/(2v_4)).$$

The parameters used in our simulations are $\phi = 0.333, g_l = 0.5, g_K = 2,\ g_{Ca} = 1,$ $v_1 = -0.01, v_2 = 0.15, v_3 = 0.1, v_4 = 0.145, v_{Ca} = 1, v_K = -.7, v_L = -0.5, I = 0.08.$

A.2. Cable equations. We derive the continuum model for a passive cable here. Consider the discrete compartment model in Figure A.1, where

$$r_j = 2\frac{R_i}{\pi d_j^2}\Delta,$$

$$R_j = \frac{R_m}{\pi d_j \Delta},$$

$$C_j = C_m \pi d_j \Delta.$$

Here Δ is the compartment length; $R_i, C_m,$ and R_m are fixed geometry independent constants; and d_j is the diameter of the jth compartment. The equations for the jth potential are

$$C_j \frac{dv_j}{dt} + \frac{v_j}{R_j} = \frac{v_{j+1} - v_j}{r_{j+1} + r_j} - \frac{v_j - v_{j-1}}{r_{j-1} + r_j}.$$

Substituting the values above into this, we obtain

$$R_m C_m \frac{dv_j}{dt} + v_j = \frac{R_m}{2R_i \Delta^2} \left(\frac{v_{j+1} - v_j}{d_j/d_{j+1}^2 + 1/d_j} - \frac{v_j - v_{j-1}}{d_j/d_{j-1}^2 + 1/d_j} \right).$$

To proceed to the continuum limit, we let $v_j = v(j\Delta)$ and $d_j = d(j\Delta)$ so that, e.g., $v_{j+1} = v(x) + \Delta v_x + \Delta^2/2 v_{xx} + \cdots$. Substituting the analogous quantities for v_{j-1} and $d_{j\pm1}$ and expanding in Δ we obtain the equation

$$R_m C_m \frac{\partial v}{\partial t} + v = \frac{R_m}{4R_i} \left(d(x)\frac{\partial^2 v}{\partial x^2} + 2d'(x)\frac{\partial v}{\partial x} \right) + O(\Delta^2).$$

Taking the limit as $\Delta \to 0$ we obtain the desired equation.

Remarks. 1. For an excitable cable, replace the resistive current with the expression for the nonlinear ionic currents.

2. If, instead of a changing diameter, we simply let r_j be a function of j to mimic a conductance alteration, the analogous operator is $(v(x)_x/r(x))_x/2$.
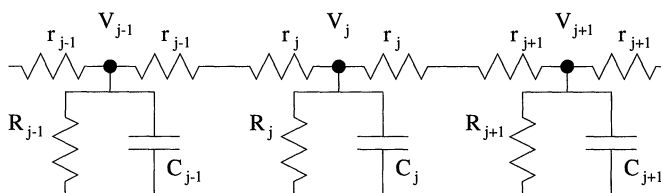
FIG. A.1. *Diagram of the cable with varying resistances.*

REFERENCES

[1] C. ANTZELEVITCH, J. JALIFE, AND G. K. MOE, *Characteristics of reflection as a mechanism of reentrant arrhythmias and its relationship to parasystole*, Circulation, 61 (1980), pp. 182–191.

[2] S. M. BAER, J. RINZEL, AND H. CARRILLO, *Analysis of an autonomous phase model for neuronal parabolic bursting*, J. Math. Biology, 33 (1995), pp. 309–333.

[3] W. H. CALVIN, J. D. LOESER, AND J. F. HOWE, *A neurophysiological theory for the pain mechanism of tic douloureux*, Pain, 3 (1977), pp. 147–154.

[4] Y. CHAGNAC-AMITAI AND B. W. CONNORS, *Horizontal spread of synchronized activity and its control by GABA-mediated inhibition*, J. Neurophys., 61 (1989), pp. 747–758.

[5] T. R. CHAY, *Studies on reentrant arrhythmias and ectopic beats in excitable tissue by bifurcation analysis*, J. Theoret. Biol., 155 (1992), pp. 137–171.

[6] E. DOEDEL, *AUTO: A program for the automatic bifurcation analysis of autonomous systems*, Congr. Numer., 30 (1981), pp. 265–284.

[7] N. FENICHEL, *Geometric singular perturbation theory for ordinary differential equations,* J. Differential Equations, 31 (1979), pp. 53–98.

[8] G. B. ERMENTROUT AND J. RINZEL, *One dimensional target patterns: Empirical stability tests*, J. Math. Biol., 10 (1980), pp. 97–100.

[9] ———, *Waves in a simple excitable or oscillatory reaction-diffusion model*, J. Math. Biol., 11 (1981), pp. 269–294.

[10] S. S. GOLDSTEIN AND W. RALL, *Changes of action potential shape and velocity for changing core conductor geometry*, Biophys. J., 14 (1974), pp. 731–757.

[11] J. F. HOWE, W. H. CALVIN, AND J. D. LOESER, *Impulses reflected from dorsal root ganglia and from focal nerve injuries*, Brain Research, 116 (1976), pp. 139–144.

[12] A. L. HODGKIN AND A. F. HUXLEY, *A quantitative description of membrane current and its application to conduction and excitation in nerve*, J. Physiol. (London), 117 (1952), pp. 500–544.

[13] H. ITO AND L. GLASS, *Theory of reentrant excitation in a ring of cardiac tissue*, Phys. D., 56 (1992), pp. 84–106.

[14] J. JALIFE AND G. K. MOE, *Excitation, conduction, and reflection of impulses in isolated bovine and canine cardiac Purkinje fibers*, Circ. Res., 49 (1981), pp. 233–247.

[15] J. P. KEENER, *Propagation and its failure in coupled systems of discrete excitable cells*, SIAM J. Appl. Math., 47 (1987), pp. 556–572.

[16] B. I. KHODOROV, *The Problem of Excitability; Electrical Excitability and Ionic Permeability of the Nerve Membrane*, New York, Plenum, 1974.

[17] N. KOPELL AND L. N. HOWARD, *Target patterns and horseshoes from a perturbed central-force problem: Some temporally periodic solutions to reaction-diffusion equations*, Stud. Appl. Math., 64 (1981), pp. 1–56.

[18] C. MORRIS AND H. LECAR, *Voltage oscillations in the barnacle giant muscle fiber*, Biophys. J., 35 (1981), pp. 193–213.

[19] F. RAMON, R. W. JOYNER, AND J. W. MOORE, *Propagation of action potentials in inhomogeneous axon regions*, Federation Proc., 34 (1975), pp. 1357–1363.

[20] J. RINZEL, *Mechanisms for nonuniform propagation along excitable cables*, in Mathematical Approaches to Cardiac Arrhythmias, Ann. New York Acad. Sci. 591, J. Jalife, ed., New York Academy of Sciences, New York, 1990, pp. 51–61.

[21] A. SHERMAN AND J. RINZEL, *Rhythmogenic effects of weak electrotonic coupling in neuronal models*, Proc. Natl. Acad. Sci. USA, 89 (1992), pp. 2471–2474.

[22] J. RINZEL AND G. B. ERMENTROUT, *Analysis of neural excitability and oscillations*, in Methods in Neuronal Modeling: From Synapses to Networks, C. Koch and I. Segev, eds., MIT Press, Cambridge, MA, 1989.

[23] G. J. ROZANSKI, J. JALIFE, AND G. K. MOE, *Reflected reentry in nonhomogeneous ventricular muscle as a mechanism of cardiac arrhythmias*, Circulation, 69 (1984), pp. 163–173.

[24] H. R. WILSON AND J. D. COWAN, *Excitatory and inhibitory interactions in localized populations of model neurons*, Biophys. J., 12 (1972), pp. 1–24.

[25] A. T. WINFREE, *The Geometry of Biological Time*, Springer-Verlag, Berlin, 1980.

[26] Y. ZHOU AND J. BELL, *Study of propagation along nonuniform excitable fibers*, Math. Biosci., 119 (1994), pp. 169–203.